Journal of Hazardous Materials 170 (2009) 836–844

Contents lists available at ScienceDirect

Journal of Hazardous Materials

journal homepage: www.elsevier.com/locate/jhazmat

Removal of Reactive Red 195 from aqueous solutions by adsorption on the surface of TiO_2 nanoparticles

V. Belessi[a,b,*], G. Romanos[a,c], N. Boukos[a], D. Lambropoulou[d], C. Trapalis[a,**]

[a] Institute of Materials Science, NCSR "Demokritos", 153 10 Aghia Paraskevi Attikis, Athens, Greece
[b] Department of Food Technology, Technological Educational Institution of Athens, Agiou Spyridonos Street, 122 10 Egaleo, Athens, Greece
[c] Institute of Physical Chemistry, NCSR "Demokritos", 153 10 Aghia Paraskevi Attikis, Athens, Greece
[d] Environmental Pollution Control Laboratory, Chemistry Department, Aristotle University of Thessaloniki, 541 24 Thessaloniki, Greece

ARTICLE INFO

Article history:
Received 30 January 2009
Received in revised form 7 May 2009
Accepted 12 May 2009
Available online 19 May 2009

Keywords:
TiO_2 nanoparticles
Reactive azo dye
Adsorption
Kinetic models

ABSTRACT

Nanoparticles of TiO_2 were synthesized and characterized by XRD, BET, TG/DTA and TEM measurements. The commercial azo dye Reactive Red 195 (RR195) was selected as a model dye in order to examine the adsorption capacity of TiO_2 at room temperature, under dark conditions. It was demonstrated that RR195 could be efficiently adsorbed in aqueous suspension of TiO_2. A study on the effects of various parameters like initial pH, concentration of dye and concentration of adsorbent has been carried out in order to find optimum adsorption conditions. The optimum pH of sorption was 3. Substantial reduction of COD, besides removal of colour, was also achieved. The experimental data were analyzed by the Langmuir and Freundlich adsorption models. Equilibrium data fitted very well with the Langmuir model signifying the energetic homogeneity of TiO_2 surface adsorption sites. At the temperature of 30 °C, the maximum monolayer adsorption capacity obtained from the Langmuir model is ~87 mg/g (pH 3.0). Kinetic studies were carried out and showed a rapid sorption of dye in the first 30 min while equilibrium was reached at 1 h. Three kinetic adsorption models were used to describe the kinetics data, the pseudo-first-order model, the pseudo-second-order model and the intraparticle diffusion model. The sorption kinetics of dye was best described by the pseudo-second-order kinetic model.

1. Introduction

Reactive dyes represent an important portion of the commercial synthetic dyes, mainly because of their excellent binding ability initiated by the formation of a covalent bond between their reactive groups and the surface groups of the textile fibers. They are used extensively in textile industries, and their release in the ecosystem represents increasing environmental danger, nowadays, because of their toxicity, mutagenicity and non-biodegradability [1–5]. Reactive dyes are, in general, the most problematic among other dyes, as they tend to pass through conventional treatment systems unaffected [5,6]. The decolourization of dye effluents has received increasing attention, thus various chemical, physical and biological treatment methods have developed for the removal of dyes from aqueous solutions, including precipitation, coagulation–flocculation, reverse osmosis, oxidation with ozone, chlorine or hydroxen peroxide, use of anion exchange membranes and bacterial cells [7–9].

Adsorption has proven to be a reliable treatment methodology due to its low capital investment cost, simplicity of design, ease of operation and insensitivity to toxic substances, but its application is limited by the high price of some adsorbents and the large amounts of wastewater normally involved. Activated carbon [10,11], mesoporous carbon [2], clay minerals [12], hydrotalcite [6], biopolymers such as chitosan beads [13] and quaternary chitosan [4] and agricultural by-products [14,15] are a few of the adsorptive materials that have been tested for the treatment of wastewaters. Adsorption onto oxides has been found to be important for metals [16,17], for organic acids [18] and for dyes [19,20]. Nevertheless, the ineffectiveness of the conventional methods to destroy pollutants such as dyes has led to the development of other efficient wastewater treatment processes such as advanced oxidation processes (AOPs) [1,21]. TiO_2 is the most commonly used effective photocatalyst for such environmental applications [21] and its adsorption capacity is a very important factor in heterogeneous photocatalysis because it determines the degradation rates. In most cases, the enhanced photoactivity of semiconductors has attributed to their superior adsorption capacity [22].

The aim of this work is to study the structure of synthesized TiO_2 nanoparticles using several techniques and to estimate their

* Corresponding author at: Institute of Materials Science, NCSR "Demokritos", 153 10 Aghia Paraskevi Attikis, Athens, Greece. Tel.: +30 2106503343; fax: +30 2106519430.
** Corresponding author.
E-mail addresses: vbelessi@teiath.gr, v.belessi@yahoo.com (V. Belessi), trapalis@ims.demokritos.gr (C. Trapalis).

0304-3894/$ – see front matter © 2009 Published by Elsevier B.V.
doi:10.1016/j.jhazmat.2009.05.045

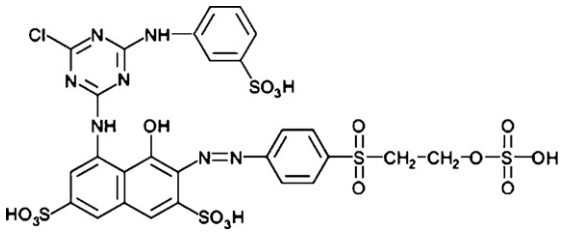

Fig. 1. Chemical structure of Reactive Red 195.

adsorption capacity for the commercial azo dye Reactive Red 195. In Fig. 1 the chemical structure of Reactive Red 195 is presented. In order to investigate the mechanism of adsorption process, three kinetic models were applied to fit the transient state experimental data, the pseudo-first-order model, the pseudo-second-order model and the intraparticle diffusion model. Furthermore, an optimization of the kinetics of the process was attempted through tuning a series of parameters such as catalyst concentration, dye concentration and initial pH. The sorption capacity and kinetics were studied using the batch method.

2. Materials and methods

2.1. Materials

Triblock copolymer poly(ethylene glycol)-block-poly(propylene glycol)-block-poly(ethylene glycol) (Mr = 8400, $(C_3H_6OC_2H_4)_x$, Aldrich), titanium butoxide (98 +%, Alfa), absolute ethanol, HNO_3 (65%, Carlo Erba). The commercial azo dye with Colour Index Generic Name Reactive Red 195 (Trade name: Triactive Red 3BS 150%, $C_{27}H_{18}O_{16}N_7S_5ClNa_4$ FW = 983.5) was supplied by Chromatourgia Tripoleos S.A. a dye manufacturer of Greece and used without further purification.

2.2. Preparation of TiO_2 nanoparticles

The TiO_2 nanoparticles were prepared as follows: 9 g of triblock copolymer poly(ethyleneglycol)-block-poly(propyleneglycol)-block-poly(ethyleneglycol) and 22 mL of titanium butoxide were dissolved in 50 mL of absolute ethanol. After the solution was vigorously stirred for 1 h, 2 mL of HNO_3 was added into the solution. The resulting suspension was stirred for 30 min, followed by the addition of 100 mL of deionized water. The powder was obtained after slow vaporization of water and ethanol. The as prepared sample was calcined at 450 °C for 1 h with a heating rate of 10 °C/min. The above protocol is a modification of the synthesis described by Yu et al. [23].

2.3. Characterisation of TiO_2 nanoparticles

X-ray powder diffraction (XRD) patterns were recorded using a D-500 Siemens diffractometer with a secondary graphite monochromator and Cu Kα radiation (λ = 1.5418 Å). The average particle sizes of anatase and brookite were calculated according to the Scherrer equation using the full widths at half-maximum (FWHM) data of each phase [24]. The mass fraction of brookite was calculated according to Eq. (1) [24], where A_A and A_B represent the integrated intensity of the anatase (1 0 1) and brookite (1 2 1) peaks, respectively.

$$W_B = \frac{2.721A_B}{2.721A_B + 0.886A_A} \quad (1)$$

Thermal analysis measurements were conducted under airflow with a heating rate of 10 °C/min on a PerkinElmer Thermogravimetric/Differential Temperature Analyser. Surface area and porosity were defined by N_2 adsorption–desorption porosimetry (77 K) using a Quantachrome (Autosorb-1, MP) porosimeter. Before measurement the sample was degassed at 350 °C and 10^{-5} mbar for 24 h. The particle size and morphology of TiO_2 nanoparticles were evaluated from TEM micrographs using a FEI CM20 microscope operated at 200 kV and characterized by a point-to-point resolution of 2.7 Å. Before measurements the sample were dispersed in ethanol and the suspensions were treated in ultrasound for 10 min. Following, a drop of very dilute suspension was placed on a carbon-coated grid and allowed to dry by evaporation at ambient temperature.

2.4. Adsorption experiments

All batch adsorption experiments were carried out under dark conditions at the temperature of 30 °C. The variation of the RR195 concentration versus time in the supernatant aliquot has been observed under various conditions such as initial pH (3, natural and 9), initial dye concentration (10, 15, 20, 25, 30, 35 and 50 mg/L) and adsorbent amount (0.02, 0.06 and 0.20 g). A stock solution of RR195 dye was prepared in 50 mg/L concentration and then diluted to the appropriate concentration. Dye concentration was calculated from the calibration curve. The initial pH was adjusted to the required value with small amounts of H_2SO_4 or NaOH solutions before mixing with the TiO_2. Adsorption was achieved by adding a known amount of adsorbent into 100 mL of dye solution of known concentration and pH, and the mixture was shaken in a thermostat bath to control the temperature at 30 ± 1 °C.

Samples were taken at predetermined time intervals, centrifuged at 10,000 rpm (7826 × *g*) for 3 min and the analysis of dye remaining in the solution was done colourimetrically using a UV-2100 Shimatzu spectrophotometer. The absorbance value for RR195 was read at 542 nm. The calibration graph of absorbance versus concentration obeyed a linear Beer–Lambert relationship. The effect of pH of the dye solution over the calibration graph was studied but no significant deviation was observed. The adsorption yield (%), the adsorbed dye amount onto the TiO_2 nanoparticles (mg/g) at any time Q_t and at equilibrium Q_{eq} were calculated from the following Eqs. (2–4), respectively:

$$\text{Adsorption yield}\,(\%) = \frac{C_0 - C_t}{C_0}100 \quad (2)$$

$$Q_t\,(\text{mg/g}) = \frac{C_0 - C_t}{M}V \quad (3)$$

$$Q_{eq}\,(\text{mg/g}) = \frac{C_0 - C_{eq}}{M}\,V \quad (4)$$

where C_0, C_t and C_{eq} are the initial, at any time t and equilibrium dye concentration (mg/L) in the dark, V is the solution volume (L) and M is the adsorbent mass (g).

Chemical oxygen demand (COD) was measured with Merck® Spectroquant kits (ref: 1.14540.0001); digestions were performed at 148 °C in a Thermoreaktor CR 3000 (Wissenschaftlich-TechnischeWerkstatten GmbH & Co., KG (WTW), Weilheim, Germany) and a Spectroquant Photolab S12 (WTW) was used for the photometric determination.

3. Results and discussion

3.1. Characterization of TiO_2 nanoparticles

The XRD pattern of the prepared TiO_2 nanoparticles is depicted in Fig. 2. The strongest peak at $2\theta = 25.2°$ arises from the (1 0 1) anatase phase reflection. Applying the Debye–Scherrer formula to this reflection, the size of TiO_2 crystallites was estimated 8 nm. The characteristic small peak at $2\theta = 30.7°$ corresponds to the

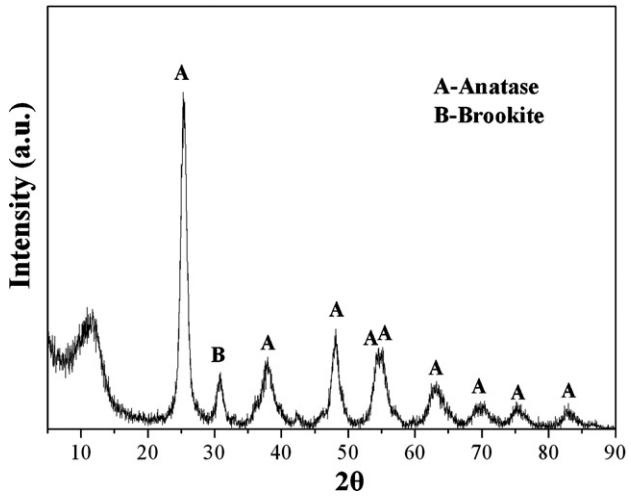

Fig. 2. XRD pattern of the prepared TiO_2 nanoparticles.

(1 2 1) diffraction peak of brookite phase. The calculated content of brookite in the sample is 23.2% according to the Eq. (1) and the size of brookite crystallites was estimated 9 nm.

In Fig. 3 the TG/DTA curve of the prepared TiO_2 nanoparticles is illustrated. The large exothermic peak at the temperature range of 260–345 °C is due to the combustion of the organic copolymer and to dehydroxylation process of titania. Also, the weak but well-defined exothermic peak, centered at about 360 °C without weight loss, indicates that a phase transformation of anatase to brookite has occurred. The TG curve shows that the decomposition process in air was completed at ≈420 °C with a mass loss of 64% in the temperature interval of 30–420 °C.

Zhang and Banfield [24] observed a phase transformation of anatase to brookite at 325 °C, without formation of rutile, using titania samples consisting of nanocrystalline anatase (46.7 wt%, 5.1 nm) and brookite (53.3 wt%, 8.1 nm). In accordance with our results, this was followed by a reaction of brookite to anatase at 350 °C, and then by conversion of anatase to brookite. The same authors have also referred that the activation energy of the anatase to brookite transformation is smaller (11.9 kJ/mol) than the activation energy of the brookite to rutile transformation (163.8 kJ/mol). These thermodynamic data explain why the transformation of anatase to brookite can proceed at lower temperatures. Furthermore, for general titania samples, the transformation sequence among anatase and brookite depends on the initial particle sizes of anatase and

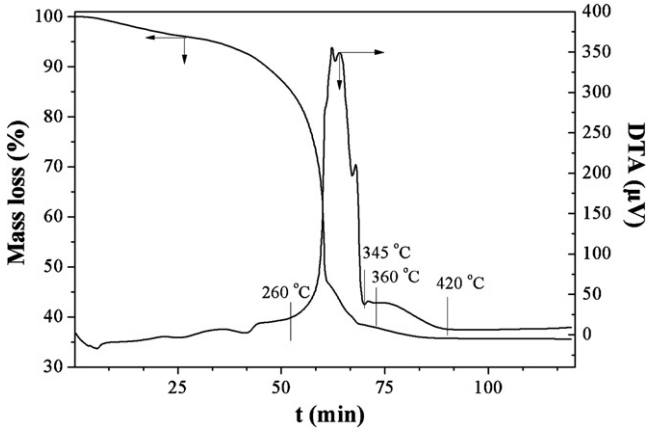

Fig. 3. TG-DTA curves of the TiO_2 nanoparticles.

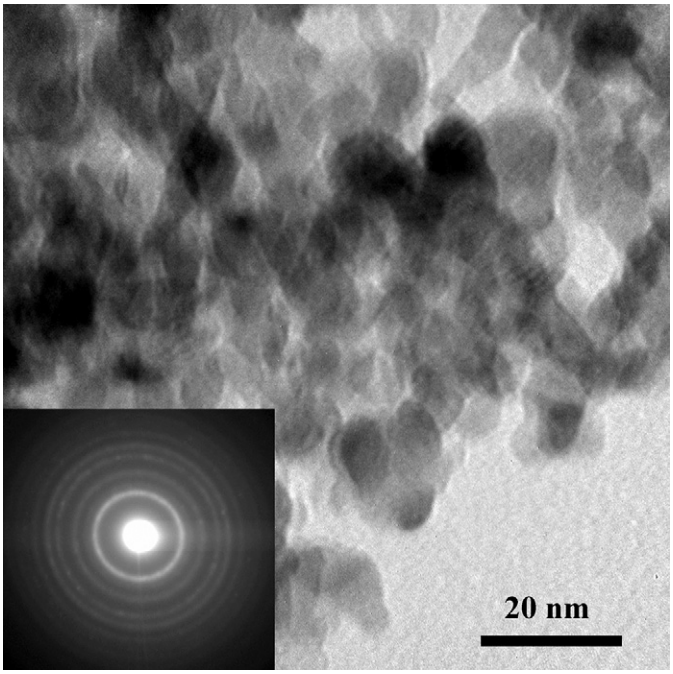

Fig. 4. Representative TEM bright field micrograph.

brookite, since particle sizes determine the thermodynamic phase stability at ultrafine sizes [24].

The morphology of the TiO_2 nanoparticles can be seen in the representative TEM bright field micrograph of Fig. 4. Their mean size is ~8.8 nm ranging between 5 and 15 nm. The corresponding selected area electron diffraction pattern is shown in the inset, indicating the presence of anatase phase, while the faint second ring corresponds to the brookite phase in agreement with the XRD results.

The morphological characterization was performed by N_2 (77 K) adsorption–desorption. The BET method was applied to determine the specific surface area (155 m^2/g) and the Barrett–Joyner–Halenda (BJH) method for the pore diameter estimation. The adsorption isotherm and the derived pore size distributions are illustrated in Fig. 5. As it is evident, the sample presents a quite extended mesopore structure with a total pore volume of about 350 cm^3(STP)/g (0.54 mL/g). This pore volume is mainly generated by the interstitial space between adjacent TiO_2 nanoparticles and

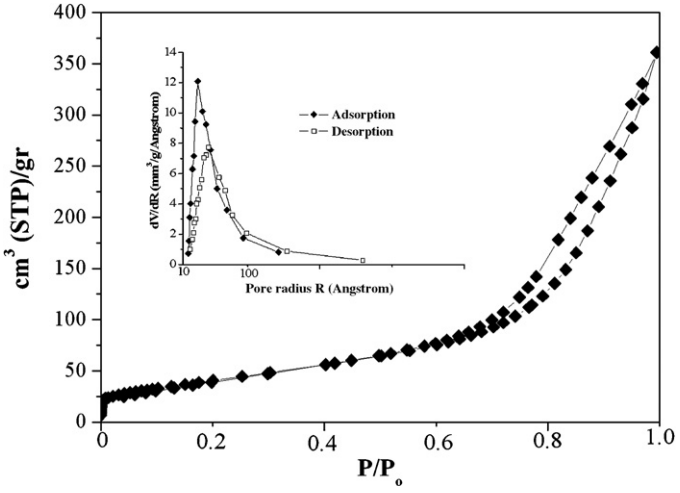

Fig. 5. Nitrogen adsorption/desorption isotherms and the corresponding pore size distribution curves (inset) for the prepared TiO_2 sample.

its high value reflects the open mesoporous architecture and large surface area of the final material. Moreover, as indicative by the steep increase of the isotherm at low relative pressures ($P/P_0 < 0.01$) a significant amount of micropores (25 cm^3(STP)/g) also exists in the sample as the result of inter-crystallite voids in each nanoparticle. The mean mesopore size estimated by the desorption branch of the N_2 (77 K) isotherm with the BJH method (inset Fig. 5) is about 9 nm, which give rise to a particle size of about 22 nm if we take into account the results of process-based models employed for the generation of random sphere packs. These models predict a ratio of 2.5 between the particle size and interparticle pore space [25]. Agglomeration of the crystallites during calcinations is the cause for the nanoparticles formation of the order of 22 nm. The presence of the triblock copolymer that slowly decomposes during the thermal treatment may act as a protective agent inhibiting the formation of larger nanoparticles and as a result the produced sample presents higher surface area (155 m^2/g) and pore volume (0.54 mL/g) than this referred in the recent literature for titania samples calcined at 450 °C [26,27]. The open mesoporous architecture in combination with the quite significant micropore structure play an important role for the effective adsorption of the RR195 dye as will be shown in the following paragraphs.

3.2. Adsorption behaviour

3.2.1. The effect of initial pH on the adsorption capacity

Undoubtedly, the surface charge of TiO_2 is highly dependent on the solution pH because of its amphoteric nature affecting its adsorption capacity and subsequently the photocatalytic oxidation to take place [19,28]. The pH at which the zeta potential equals zero is called the isoelectric point (IEP) and it can be used to qualitatively assess the adsorbent surface charge. The empirical isoelectric point, pH_{iep}, of TiO_2 reported in the literature ranges from 2 to 8.9 [28–31]. However, the pH_{iep} for the Degussa P25 TiO_2 is ranged between 6.2 and 6.9 [19,30,31]. Note, however that the broad range of pH_{iep} for TiO_2 nanoparticles depends on phase, method, preparation, hydration of the material and ionic strength of the solution [18,29–31].

In Fig. 6 the effect of initial pH on the adsorption yield (%) of RR195 onto TiO_2 at 30 °C after 3 h equilibration, for adsorbent concentration 2.0 and 0.2 g/L and initial dye concentration 50 mg/L is depicted. It is obvious that the adsorbed amount of RR195 dye increased with decreasing initial pH. Reactive dyes have anionic character, so the higher uptake values obtained at lower pH values are due to electrostatic attractions between the negatively charged dye anion and the positively charged TiO_2 ($pH < pH_{iep}$) according to Eq. (5) [1,15,28]. It appears that Ti^{IV}–OH_2^+ could be responsible for the dye adsorption on titanium oxide surface, suggesting that electrostatic attraction leads to the observed adsorption [1,28,30]. At this point, it should be mentioned that in addition to pH, which strongly influences adsorption, the coverage of the surface is significantly affected by the potential of the interfacial region. Thus, the accumulation of the negatively charged ions of the RR195 in this region causes the development of a negative charge, which inhibits further adsorption of the ions of the dye [19]. On the contrary, as the initial pH of the solution increases, the number of the negatively charged surface sites on the adsorbent increases and does not favour the adsorption of dye anions due to the repulsive electrostatic forces ($pH > pH_{iep}$) according to Eq. (6).

$$Ti^{IV}\text{–}OH + H^+ \rightarrow Ti^{IV}\text{–}OH_2^+, \; pH < pH_{iep} \quad (5)$$

$$Ti^{IV}\text{–}OH + OH^- \rightarrow Ti^{IV}\text{–}O^- + H_2O, \; pH > pH_{iep} \quad (6)$$

Summarizing, pH influences both the surface state of TiO_2 and the ionization state of azo dye explaining the strong adsorption of RR195 at pH 3 in accordance with other studies [1,19].

Particularly, after 2 h contact time that equilibrium has established and for pH solution values 3, 6.5 (natural) and 9, the adsorption yields that have attained are 38%, 0.5% and 0%, respectively, for adsorbent concentration 0.2 g/L and initial dye concentration 50 mg/L (Fig. 7a). For 10-fold increase in adsorbent concentration (2.0 g/L) and for constant dye concentration, the adsorption yields that have established for pH solution values 3, 6.5 and 9 are 100%, 1.5% and 0.3%, respectively (Fig. 7b).

In accordance with our results, Bourikas et al. [19], have reported that the extent of adsorption of the Acid Orange 7 on the TiO_2 sur-

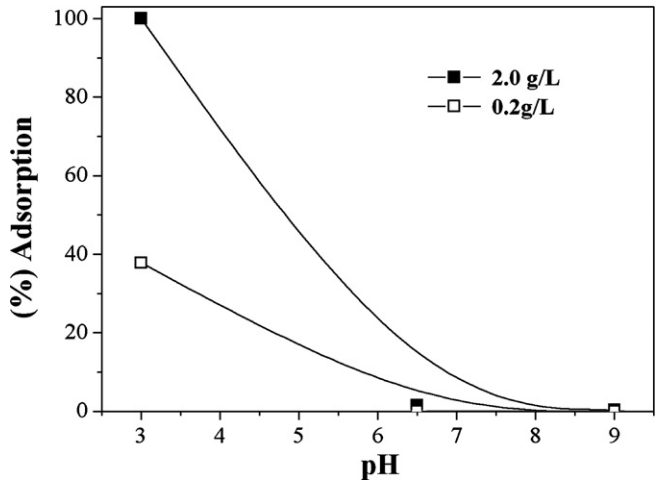

Fig. 6. Effect of initial pH on the adsorption of RR195 dye on TiO_2 for adsorbent concentration 2.0 and 0.2 g/L. Conditions: temperature 30 °C, initial dye concentration 50 mg/L, contact time 3 h.

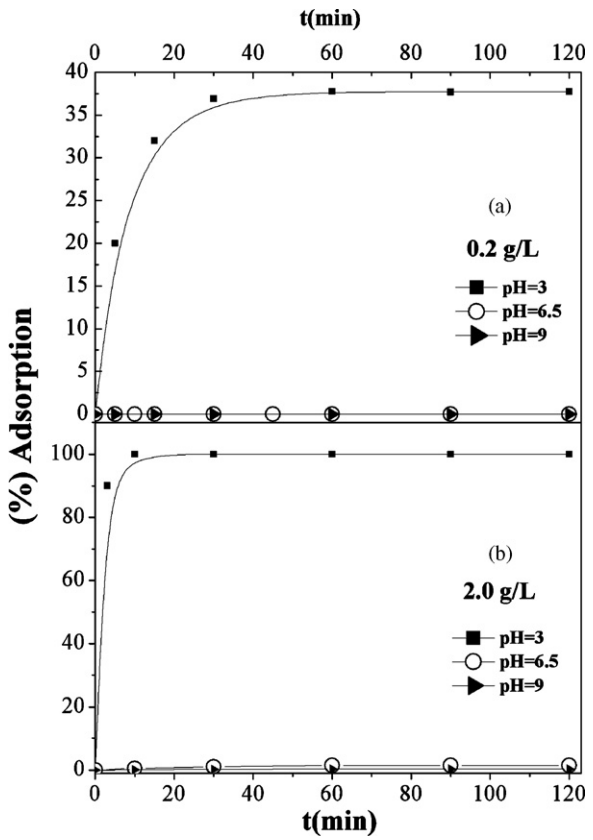

Fig. 7. The effect of contact time and pH on the adsorption of RR195 dye on TiO_2 for adsorbent concentration (a) 0.2 g/L and (b) 2.0 g/L. Conditions: temperature 30 °C, initial dye concentration 50 mg/L and contact time 2 h.

face decreases rapidly with increasing pH and becomes negligibly small at pH 10. Furthermore, it was demonstrated that the adsorption of the azo dye on titanium oxide occurs to a significant extent only at pH values lower than 7, via the sulfonic group of the azo dye, through the formation of a bidentate innersphere surface complex. Also, in a remarkable study Dunphy-Guzman et al. [32] investigated the aggregation of different polymorphs of TiO_2 nanoparticles as a function of pH. The results of their study showed very stable, dispersed suspensions of TiO_2 nanoparticles at pH 1 and 12 due to the presence of an electric double layer, as these pH values are far from the isoelectric point for TiO_2. When the pH was altered so that it approached the pH_{iep} of the phases considered, the repulsive forces between nanoparticles decreased, causing the TiO_2 nanoparticles to aggregate. It is possible, therefore, at near neutral pH 6.5, particle aggregation and its influence on reactive surface area may also be impacting the dye uptake we have observed for TiO_2 nanoparticles. The same authors also found that nanoparticle aqueous suspensions were more stable at extremely acidic pH values rather than extremely basic pH values, which they interpreted as evidence that TiO_2 nanoparticles are less capable of holding negative surface charge. On the basis of such considerations, the influence of pH in controlling the stability of TiO_2 suspensions impacts the surface adsorption and reactivity of nanoparticles [18,32].

3.2.2. The effect of contact time and initial dye concentration on the adsorption capacity for initial pH 3

The effect of contact time and initial dye concentration on the adsorption of RR195 dye onto TiO_2 particles, at 30 °C, was investigated in the range of 10–75 mg/L for adsorbent concentration 2.0 g/L (Fig. 8a) and in the range of 10–50 mg/L for adsorbent concentration 0.2 g/L (Fig. 8b). The larger amount of dye was rapidly removed in the first 20 min of contact time while the adsorption equilibrium for

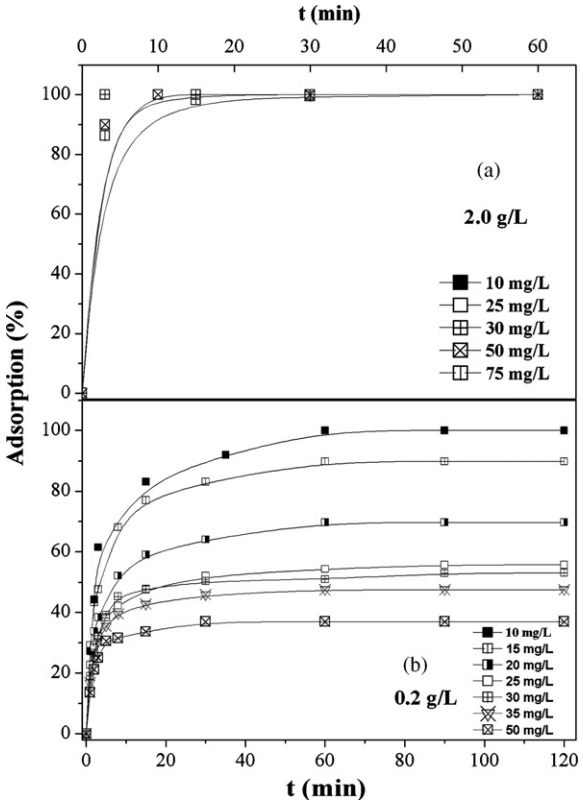

Fig. 8. The effect of contact time and initial dye concentration on RR195 removal by TiO_2 for adsorbent concentration (a) 2.0 g/L and (b) 0.2 g/L. Conditions: temperature 30 °C, pH 3 and contact time 2 h.

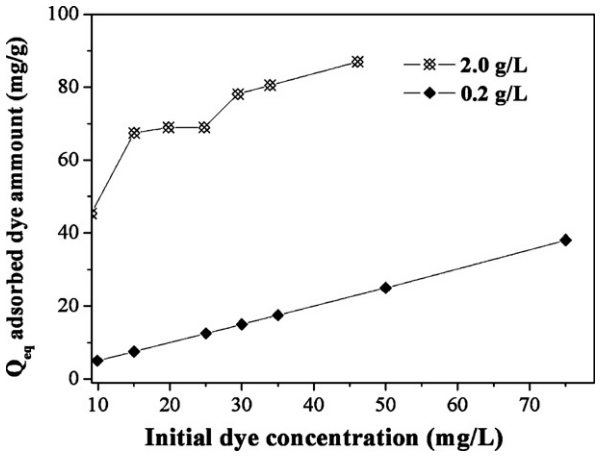

Fig. 9. The effect of initial dye concentration (mg/L) and adsorbent dosage (g/L) on the adsorbed dye amount at equilibrium (mg/g). Conditions: temperature 30 °C, pH 3 and contact time 2 h.

the studied dye was established after 60 min, independently on the initial dye concentration [20]. This short duration of the present experiments implies that sorption of colour is a kinetic rather a diffusion-controlled process [6]. Also, the rapid kinetics has significant practical importance, as it will facilitate smaller reactor volumes ensuring efficiency and economy [14].

In particular, for adsorbent concentration 2.0 g/L (Fig. 8a), the adsorption yield of RR195 onto TiO_2 nanoparticles is ~100%, after 15 min of contact time and for different initial dye concentrations 10–75 mg/L. In previous studies, this acute jump at the beginning of sorption has been considered as indicative of a fast initial external mass transfer step [33]. It is expected that external mass transfer resistance in the aqueous phase is negligible, which is reasonable in well-shaken adsorption systems. Furthermore, Lazaridis et al. [6], supported that such an extraordinary fast rate of initial colour removal may also manifest a fast chemical ion surface attachment. For the same pH value and changing the load by one order of magnitude (adsorbent concentration 0.2 g/L) a decrease in adsorption yield appeared (Fig. 8b). Specifically, the adsorption yields (%) of TiO_2 after 60 min of contact time and for initial dye concentrations of RR195 dye 10, 15, 20, 25, 30, 35 and 50 mg/L were found as 100%, 89.8%, 69.7%, 55.7%, 52.9%, 47.5% and 37.8%, respectively. As far as concern, the observed lower adsorption yields at higher dye concentrations are due to the saturation of adsorption sites on TiO_2. Generally, the as prepared porous TiO_2 was effectively capable to remove the reactive dye in solutions of a wide region of dye concentration completely.

Fig. 9 shows the variation of the adsorbed dye amount at equilibrium (mg/g) versus initial dye concentration (mg/L). For adsorbent concentration 2.0 g/L, the adsorbed RR195 amount was enhanced as the initial concentration of the dye increased from 10 to 75 mg/L in accordance with previous studies [3,13,15,34,35]. Similarly, for adsorbent concentration 0.2 g/L, the dye uptake increased with increasing initial dye concentration from 10 to 20 mg/L but then did not vary very much with further increase in initial dye concentration.

Summarizing we observe that enhancing the initial dye concentration, the percentage colour removal decreased while the amount of dye adsorbed per unit of adsorbent mass enhanced.

3.2.3. The effect of the adsorbent concentration

The adsorption of the RR195 dye investigated as a function of adsorbent concentrations in a solution of pH 3.0, at 30 °C and for initial dye concentration 50 mg/L (Fig. 10). The adsorption yield (%) of TiO_2 for RR195 is 100%, 89.2% and 37.8% for 2.0, 0.6 and 0.2 g/L of

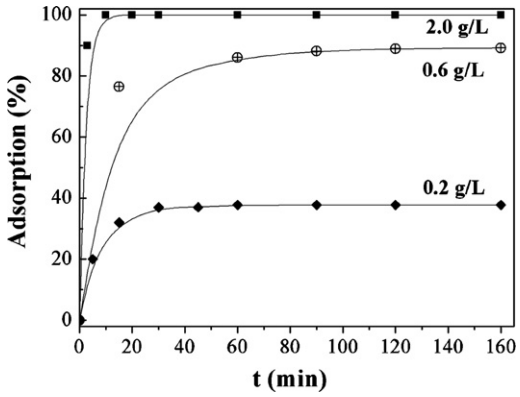

Fig. 10. Effect of contact time and adsorbent dose on RR195 removal by TiO_2 nanoparticles. Conditions: temperature 30 °C, dye concentration 50 mg/L and pH 3.

adsorbent dose, respectively. This means that the adsorption yield increased with increasing adsorbent dose (Figs. 10, 7a and b) and this is directly proportional to the external surface area of the sorbent [6]. On the other hand, the adsorption capacity (amount of dye adsorbed per unit of adsorbent weight) is 25, 66.48 and 86.98 mg/g for 2.0, 0.6 and 0.2 g/L of adsorbent dose, respectively (data not shown). The decrease in adsorption capacity with an increase in the adsorbent concentration could be ascribed to the fact that some of the adsorption sites remained unsaturated during the adsorption process [14]. Another reason may be due to the particle interactive behaviour, such as aggregation, resulted from high adsorbent dose. Such aggregation of TiO_2 nanoparticles would lead to decrease in total surface area available for adsorption and an increase in the diffusion path length [14,15]. Similar phenomena were also observed for Rhodamine 6G or methylene blue adsorption on combined TiO_2/SiO_2 mesoporous photocatalysts [36] and for Malachit Green adsorption on sawdust [37].

Summarizing, effects of parameters like initial pH, contact time, initial dye concentration and adsorbent concentration on the adsorption behaviour were studied. These are the major variables governing the efficiency of the process. However, besides the removal of colour, the reduction of COD was monitored because the former does not always confirm the latter. Specifically, COD analyses were performed at the beginning and at the end of the experiment for initial dye concentration 50 mg/L, adsorbent dose 2.0 g/L and pH 3.0 (30 °C). It was found that for the maximum decolourization efficiency (100%) the COD reduction was 81.4%. Furthermore, a blank was also prepared without adding TiO_2 nanoparticles. The change in COD value of the blank was not appreciable during isotherm experiment.

These experimental results confirm the adsorption as the removal mechanism of the dye molecule and indicate the efficiency of the adsorption method for wastewater treatment.

3.2.4. Adsorption isotherms

For the adsorption experiments, the two common adsorption isotherm models Langmuir Eqs. (7) and (9) [38] and Freundlich Eqs. (8) and (10) [39] were used to calculate the adsorption data for initial pH 3.

$$q_e = KC_e \tag{7}$$

$$q_e = K_F C_e{}^{1/n} \tag{8}$$

$$\frac{C_{eq}}{Q_{eq}} = \frac{1}{Q_{max}} C_{eq} + \frac{1}{Q_{max} K_L} \tag{9}$$

$$\log Q_{eq} = \log K_F + \frac{1}{n} \log C_{eq} \tag{10}$$

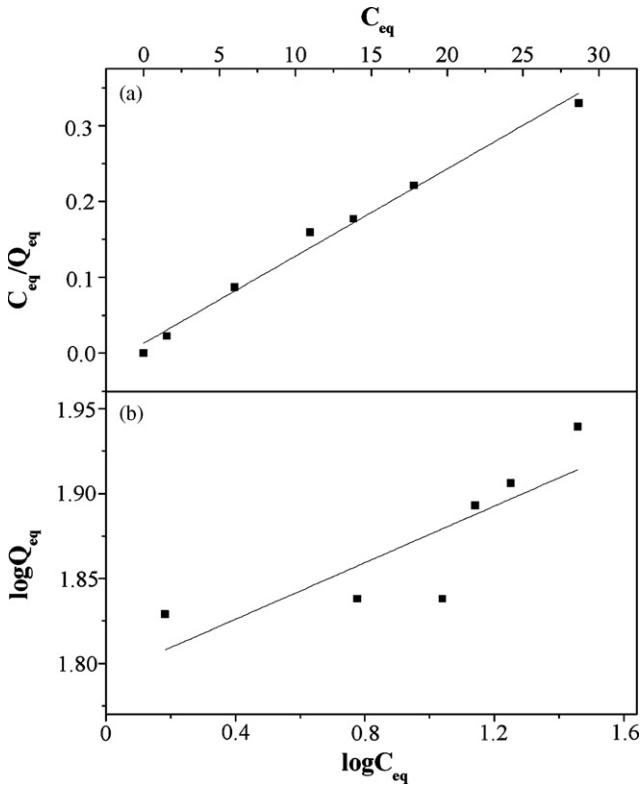

Fig. 11. Linearized Langmuir (a) and Freundlich (b) adsorption isotherms of Reactive Red 195 dye for TiO_2 nanoparticles.

where C_{eq} (mg/L) is the concentration of the dye in the solution at equilibrium, Q_{eq} (mg/g) is the adsorbed dye amount at equilibrium per unit weight of adsorbent, Q_{max} (mg/g) the maximum amount of adsorbed dye corresponding to complete monolayer coverage, K_L (L/mg) is the Langmuir adsorption equilibrium constant related to the energy of adsorption, K_F [(mg/g) (mg/L)^n] is the Freundlich adsorption equilibrium constant which is an indicator of the adsorption capacity and n is a characteristic coefficient relating to adsorption intensity.

The widely used Langmuir isotherm is fundamental in describing the interactive behaviour between solutes and adsorbent and is based on the assumption that maximum adsorption corresponds to a saturated monolayer of adsorbate molecules on adsorbent surface with a constant energy and there is no transmigration of adsorbate in the plane of adsorbent surface. The Freundlich isotherm used for isothermal adsorption is a special case for heterogeneous surface energy systems, in which the energy term in the Langmuir equation varies as a function of surface coverage strictly due to variation of the sorption.

The plot of (C_{eq}/Q_{eq}) versus C_{eq} (Fig. 11a) gives a straight line with a correlation coefficient $R^2 = 0.9871$. The Q_{max} (86.96 mg/g) and K_L (0.89 L/mg) derived values were calculated from the slope and intercept, respectively. The value of the calculated adsorption equilibrium constant K_L of TiO_2 is high and the factors that led to the enhanced adsorption capacity are related with the porous structure of the TiO_2. The plot of ($\log Q_{eq}$) versus ($\log C_{eq}$) (Fig. 11b) gives a straight line with a correlation coefficient $R^2 = 0.6016$. It is obvious that the linear adsorption model ($R^2 = 0.9871$) describes better the adsorption behaviour of RR195 on TiO_2 nanoparticles than the Freundlich model ($R^2 = 0.6016$).

K_F (62.02) and $1/n$ (0.083) were determined from the intercept and slope of the plot ($\log Q_{eq}$) versus ($\log C_{eq}$) (Fig. 11b). It was generally accepted that under a constant temperature, the n val-

Table 1
The pseudo-first, pseudo-second-order and intraparticle diffusion kinetic model constants for the adsorption of the RR195 dye onto TiO_2 sample, for different initial dye concentrations, pH 3, adsorbent dose 0.2 g/L, and temperature 30 °C.

C_0 (mg/L)	Q_{eq}, exp (mg/g)	First-order kinetic model			Second-order kinetic model			Intraparticle diffusion			
		k_1 (1/min)	$q_{1,cal}$ (mg/g)	R^2	k_2 (g/mg min)	$q_{2,cal}$ (mg/g)	R^2	$k_{d.1,cal}$ (mg/g min$^{-1/2}$)	R^2	$k_{d.2,cal}$ (mg/g min$^{-1/2}$)	R^2
10	45.30	0.0760	27.90	0.9642	0.0155	46.32	0.9949	21.0601	0.9873	3.7929	0.9623
15	67.42	0.0730	38.20	0.9142	0.0055	69.44	0.9998	15.2612	0.9649	4.1136	0.8947
20	68.95	0.0696	37.93	0.9272	0.0055	70.92	0.9970	14.0740	0.9784	4.3580	0.9098
25	68.95	0.0525	30.52	0.9311	0.0060	70.42	0.9999	13.3800	0.9766	4.4982	0.9449
30	78.12	0.0438	27.60	0.7167	0.0064	79.18	0.9998	21.1156	0.9777	2.7892	0.9747
35	80.54	0.0940	39.29	0.9272	0.0068	82.64	0.9999	25.6080	0.9575	3.9594	0.9642
50	86.98	0.1036	41.74	0.9368	0.0072	88.42	0.9999	31.2526	0.9720	4.5589	0.9989

ues increased with decreasing adsorption energy, which implied that the larger the n value, the stronger the adsorption intensity. In general, values $n > 1$ illustrated that adsorbate was favourably adsorbed on an adsorbent, while $n > 1$ indicated that adsorbate was unfavourably adsorbed on an adsorbent. The high n and K_F values suggest that the reactive dye is favourably adsorbed on the TiO_2 nanoparticles and also the easy separation of the dye from the aqueous solution. However, the correlation coefficients ($R^2 = 0.6016$) indicate that Langmuir isotherm has been fitted better for the adsorption of RR195 on TiO_2.

We should note that the calculated value of the sorption capacity Q_{max} at 30 °C (86.96 mg/g = 0.0884 mmol/g) is not high as compared with commercial activated carbons, other synthetic carbons or chitosan salts e.g. >300 mg of direct dyes per gram of sawdust carbon [10], ~350 mg of acid blue dye per gram of porous carbon [40], ~180 mg of Congo Red per gram of porous carbon [41], ~1060 mg of reactive orange 16 per gram of quaternary chitosan salt cross-linked [4]. However, if we use the Q_{max}/S_{BET} (mmol/nm) ratio in order to find the loading per unit surface area, the resulting value is 5.7×10^{-22} mmol/nm^2 for the as prepared TiO_2 nanoparticles. This value is significantly higher compared to various porous carbons reported in literature i.e. 1.90, 3.74, 3.96×10^{-22} mmol/nm^2 for Remazol Red 3BS [2]. Also, the uptake values of the TiO_2 nanoparticles are higher or compared to other TiO_2 systems reported in the literature at pH 3 i.e. ~9.47 mg of Reactive Yellow 145 per gram of SiO_2/TiO_2 [1], ~30 mg of Acid Orange 7 per gram of TiO_2-P25 [19].

3.2.5. Kinetic study

In order to investigate the mechanism of adsorption of the reactive dye on TiO_2 nanoparticles, the following kinetic models were adopted to examine the experimental data: (i) pseudo-first-order equation, (ii) pseudo-second-order equation and (iii) intraparticle diffusion model.

(i) The pseudo-first-order equation

The integrated rate law for a pseudo-first-order rate expression Eq. (11) [42,43] is given as:

$$\log(q_1 - q) = \log q_1 - \frac{k_1}{2.303} t \tag{11}$$

where q_1, q are the amounts of dye adsorbed on adsorbent at equilibrium and at time t, respectively (mg/g), and k_1 is the pseudo-first-order adsorption kinetic constant of (1/min). A straight line of $\log(q_1 - q)$ versus t suggests the applicability of this kinetic model to fit the experimental data. In the literature has stated that in many cases, the pseudo-first order model fits the experimental data well for the initial stage of the adsorption processes [42,43]. In this work, the correlation coefficients for the first-order kinetic model were low (Table 1) and the calculated q_1 values obtained from the first-order kinetic model do not give reasonable values, because they are too low compared with experimental Q_{eq} values. The calculated values k_1, q_1 and the correlation coefficients (R^2) are listed in Table 1.

(ii) The pseudo-second-order equation

The integrated rate law for the pseudo-second-order kinetic model [44] may be expressed by the following equation:

$$\frac{t}{q} = \frac{1}{k_2 q_2^2} + \frac{t}{q_2} \tag{12}$$

where k_2 (g/mg min) is the rate constant of pseudo-second-order adsorption, q_2, q are the amounts of dye adsorbed on adsorbent at equilibrium and at any time t, respectively (mg/g). Applying the second-order kinetic model it is more likely to predict the behaviour over the whole range of adsorption while chemical reaction seems significant in the rate-controlling step [44].

The q_2, k_2 values calculated from the slope and the intercept of the plot (t/q) versus t, respectively (Table 1). The correlation coefficients for the second-order kinetic model are greater than 0.9949 for all the cases (Table 1), denoting a good agreement of experimental data with the second-order kinetic model for different initial dye concentrations. Also, the calculated q_2 values agree very well with the experimental data. These results indicate that the RR195 adsorption kinetics on TiO_2 is better fitted by the pseudo-second-order kinetic model, that is based on the assumption that the rate-limiting step may be chemical sorption or chemisorption involving valency forces through sharing or exchange of electrons between sorbent (TiO_2) and sorbate (dye anions) [44]. Simiral results have reported for the adsorption of different reactive dyes onto cross-linked chitosan [13], yeasts [3], mesoporous carbons [2], cross-linked quaternary chitosan [4], wheat bran [15] and surfactant-modified zeolite [35]. According to the pseudo-second-order model, the adsorption rate dq/dt is proportional to the second-order of $(q_2 - q)$. In this work TiO_2 nanoparticles have relatively high equilibrium adsorption density q_2, which is ascribed to the fact that the RR195 can be quickly adsorbed onto the exterior large pore-structure of TiO_2. So, the equilibrium times are short indicating a high degree of affinity between the dye RR195 and the TiO_2 nanoparticles [6,13]. Furthermore, there is a tendency for rate constants k_2 to decrease with increasing initial dye concentration, which has also been reported for other adsorption systems [3,45,46]. The decrement of k_2 values means that the adsorption kinetics becomes slower as the concentration of reactive dye enhances that shows the presence of diffusion limited transport of dye. It is possible that at higher initial dye concentrations, the difference in the chemical potential is high enough to drive the diffusion of RR195 molecules through the intraparticle pores. In this case intraparticle diffusion and spontaneous interparticle chemisorption contribute simultaneously on the overall kinetics and since diffusion is a slower mechanism the rate

constants k_2 decrease. This assumption is investigated in the next section.

(iii) The Intraparticle diffusion model

The possibility of intraparticle diffusion resistance affecting adsorption was explored by using the kinetic model proposed by Weber and Morris [47] where the initial rate of intraparticle diffusion can be obtained by linearization of the curve:

$$q_t = f(t^{0.5}) \quad (13)$$

So, when the intraparticle diffusion controls the adsorption kinetics process the plot of q_t versus $t^{0.5}$ gives a straight line passing through the origin and the slope gives the rate constant k_d. Such plots may present a multilinearity, which indicates that two or more steps occur [14,34,46,48]. This model assumes that the external mass transfer resistance in the aqueous phase is negligible, which is reasonable in well-shaken adsorption systems. At this point we must note that if the adsorption process is controlled by the external resistance, the plot of $\ln C_t$ versus time should be linear [14]. In our case this kind of relation was indicated for the first 5 min of adsorption kinetic.

As far as concern the intraparticle diffusion, this step occurs after the adsorbate has passed through the boundary layer and has transported through the pores to adsorption sites. The intraparticle transportation may occur by molecular diffusion through the solution in the pores (pore diffusion) or by diffusion along the adsorbent surface (surface diffusion) after adsorption takes place. From the plots of q_t versus $t^{0.5}$ (data not shown here) it is evident that there are three regions of uptakes, each being a straight line with different slope. The same behaviour has referred by Wang et al. [14] for the adsorption of two basic dyes onto agricultural by-products, by Fontecha-Camara et al. [46] for the adsorption of herbicides on activated carbons and for phenol adsorption on three apatites [34], activated bentonites [49] and activated carbon [48].

At the first stage ($t < 5$ min) a very fast uptake is observed, the second stage ($5 < t < 35$ min) is a transition stage and the third is flat ($t > 35$ min). The first stage can be attributed to a very fast adsorption of RR195 dye onto the available sites of the external surface of TiO_2 due to electrostatic attractions between the negatively charged dye anions and the positively charged TiO_2 [34]. During the second stage which is ascribed to the intraparticle diffusion, it is likely that the dye molecules began to enter the titania, via the mesopores within the nanoparticles and was adsorbed on the active sites of the adsorbent internal surface [11,14,48]. The molecules of Reactive Red 195 could not easily penetrate into the micropores (<2 nm diameter) because of their large size, so the diffusion resistance was increased and the diffusion rate reduced [11]. Finally, further decrease in dye concentration in the solution caused the diffusion rate to become constantly lower until the diffusion process reached equilibrium (stage three) [11,14,34]. Similarly, Kumar et al. [48] have reported the existence of three regions of uptakes in the typical plots of q_t versus $t^{0.5}$ and supported that the adsorbate (phenol or 4-nitrophenol) is initially transported to macro, then meso and finally slowly diffused into micropores of the granular activated carbon. Allen et al. [50] noted the similar trend for dye adsorption on peat at various initial concentrations and linked this behaviour to pore structure of the peat used.

The k_{d_1} and k_{d_2} values calculated from the slopes of the straight lines of the respective plots for the first and second stages (for different concentrations) are given in Table 1. The k_{d_3} values are almost zero and are not listed in table. As expected, the k_{d_1}, k_{d_2} and k_{d_3} values follow the order $k_{d\_1} > k_{d\_2} > k_{d\_3}$ [14]. The values of the corresponding correlation coefficients R^2 are listed in the same table. Generally, the rate constant of the intraparticle diffusion model increases with increasing initial dye concentration [11,45,46]. However, in the present study no conclusive trend for effect of concentration on the rate constant of the intraparticle diffusion can be discerned.

4. Conclusions

Mesoporous TiO_2 was prepared and the adsorption of the commercial reactive dye RR195 on the as prepared TiO_2 was studied in the liquid phase. The results showed that at acidic pH values high electrostatic attractions existed between the positively charged surface of the adsorbent and anionic dye. Optimal dye sorption occurred at pH 3. Adsorption of RR195 by TiO_2 reached equilibrium within 1 h and the results of adsorption showed that TiO_2 nanoparticles can be effectively used as a sorbent for the removal of anionic dyes in solutions of a wide region of dye concentration. The efficiencies of decolourization and COD reduction were accomplished at optimum conditions as 100% and 81.4%, respectively. The equilibrium data have been analyzed using Langmuir and Freundlich isotherms and the characteristic parameters for each isotherm have been determined. According to the correlation coefficients R^2 the Langmuir isotherm has been fitted better for the adsorption of RR195 on TiO_2. The kinetics studies of RR195 on titanium oxide nanoparticles were based on pseudo-first-order, pseudo-second-order and intraparticle diffusion rate mechanism. The data indicate that the adsorption kinetics of RR195 on TiO_2 nanoparticles followed the pseudo-second-order expression. Further analyses suggested that the sorption process is controlled by intraparticle diffusion of dye.

Acknowledgement

The authors thank the GSRT, Greek Ministry of Research and Development for financial support under the Grant 05 Non EU 247.

References

[1] A. Aguedach, S. Brosillon, J. Morvan, E.K. Lhadi, Photocatalytic degradation of azo-dyes reactive black 5 and reactive yellow 145 in water over a newly deposited titanium dioxide, Appl. Catal. B: Environ. 57 (2005) 55–62.
[2] D.D. Asouhidou, K.S. Triantafyllidis, N.K. Lazaridis, K.A. Matis, S.-S. Kim, T.J. Pinnavaia, Sorption of reactive dyes from aqueous solutions by ordered hexagonal and disordered mesoporous carbons, Micropor. Mesopor. Mater. 117 (2009) 257–267.
[3] Z. Aksu, G. Donmez, A comparative study on the biosorption characteristics of some yeasts for remazol blue reactive dye, Chemosphere 50 (2003) 1075–1083.
[4] S. Rosa, M.C.M. Laranjeira, H.G. Riela, V.T. Favere, Cross-linked quaternary chitosan as an adsorbent for the removal of the reactive dye from aqueous solutions, J. Hazard. Mater. 155 (2008) 253–260.
[5] C.I. Pearce, J.R. Lloyd, J.T. Guthrie, The removal of colour from textile wastewater using whole bacterial cells: a review, Dyes Pigments 58 (2003) 179–196.
[6] N.K. Lazaridis, T.D. Karapantsios, D. Georgantas, Kinetic analysis for the removal of a reactive dye from aqueous solution onto hydrotalcite by adsorption, Water Res. 37 (2003) 3023–3033.
[7] T. Robinson, G. McMullan, R. Marchant, P. Nigam, Remediation of dyes in textile effluent: a critical review on current treatment technologies with a proposed alternative, Bioresour. Technol. 77 (2001) 247–255.
[8] P. Cooper, Removing colour from dyehouse waste waters—a critical review of technology available, J. Soc. Dyers Colour. 109 (1993) 97–100.
[9] Y.M. Slokar, A. Majcen Le Marechal, Methods of decoloration of textile wastewaters, Dyes Pigments 37 (1998) 335–356.
[10] P.K. Malik, Dye removal from wastewater using activated carbon developed from sawdust: adsorption equilibrium and kinetics, J. Hazard. Mater. B113 (2004) 81–88.
[11] E. Demirbas, M. Kobya, M.T. Sulak, Adsorption kinetics of a basic dye from aqueous solutions onto apricot stone activated carbon, Bioresour. Technol. 99 (2008) 5368–5373.
[12] S.D. Lambert, N.J.D. Graham, C.J. Sollars, G.D. Fowler, Evaluation of inorganic adsorbents for the removal of problematic textile dyes and pesticides, Water Sci. Technol. 36 (1997) 173–180.
[13] M.-S. Chiou, H.-Y. Li, Equilibrium and kinetic modeling of adsorption of reactive dye on cross-linked chitosan beads, J. Hazard. Mater. 93 (2002) 233–248.
[14] X.S. Wang, Y. Zhou, Y. Yiang, C. Sun, The removal of basic dyes from aqueous solutions using agricultural by-products, J. Hazard. Mater. 157 (2008) 374–385.
[15] F. Cicek, D. Ozer, A. Ozer, A. Ozer, Low cost removal of reactive dyes using wheat bran, J. Hazard. Mater. 146 (2007) 408–416.

[16] Y. Gao, R. Wahi, A.T. Kan, J.C. Falkner, V.L. Colvin, M.B. Tomson, Adsorption of cadmium on anatase nanoparticles—effect of crystal size and pH, Langmuir 20 (2004) 9585–9593.
[17] M.-S. Kim, K.-M. Hong, J.G. Chung, Removal of Cu (II) from aqueous solutions by adsorption process with anatase-type titanium dioxide, Water Res. 37 (2003) 3524–3529.
[18] J.M. Pettibone, D.M. Cwiertny, M. Scherer, V.H. Grassian, Adsorption of organic acids on TiO_2 nanoparticles: effects of pH, nanoparticle size and nanoparticle aggregation, Langmuir 24 (2008) 6659–6667.
[19] K. Bourikas, M. Stylidi, D.I. Kondarides, X. Verykios, Adsorption of acid orange 7 on the surface of titanium dioxide, Langmuir 21 (2005) 9222–9230.
[20] S. Pirillo, M.L. Ferreira, E.H. Rueda, Adsorption of alizarin, eriochrome blue black R, and fluorescein using different iron oxides as adsorbents, Ind. Eng. Chem. Res. 46 (2007) 8255–8263.
[21] I.K. Konstantinou, T.A. Albanis, TiO_2-assisted photocatalytic degradation of azo dyes in aqueous solute on: kinetic and mechanistic investigations a review, Appl. Catal. B: Environ. 49 (2004) 1–14.
[22] V. Belessi, D. Lambropoulou, I. Konstantinou, R. Zboril, J. Tucek, D. Jancik, T. Albanis, D. Petridis, Structure, photocatalytic performance of magnetically separable titania photocatalysts for the degradation of propachlor, Appl. Catal. B: Environ. 87 (2009) 181–189.
[23] J.C. Yu, L. Zhang, Z. Zheng, J. Zhao, Synthesis and characterization of phosphated mesoporous titanium dioxide with high photocatalytic activity, Chem. Mater. 15 (2003) 2280–2286.
[24] H. Zhang, J.F. Banfield, Understanding polymorphic phase transformation behaviour during growth of nanocrystalline aggregates: insights from TiO_2, J. Phys. Chem. B 104 (2000) 3481–3487.
[25] M.E. Kainourgiakis, E.S. Kikkinides, Th.A. Steriotis, A.K. Stubos, K.P. Tzevelekos, N.K. Kanellopoulos, Structural and transport properties of alumina porous membranes from process-based and statistical reconstruction techniques, J. Colloid Interf. Sci. 231 (2000) 158–167.
[26] J-h. Xu, W.-L. Dai, J. Li, Y. Cao, H. Li, H. He, K. Fan, Simple fabrication of thermally stable apertured N-doped TiO_2 microtubes as a highly efficient photocatalyst under visible light irradiation, Catal. Commun. 9 (2008) 146–152.
[27] T. Horikawa, M. Katoh, T. Tomida, Preparation and characterization of nitrogen-doped mesoporous titania with high specific surface area, Micropor. Mesopor. Mater. 110 (2008) 397–404.
[28] W.-Y. Wang, Y. Ku, Effect of solution pH on the adsorption and photocatalytic reaction behaviours of dyes using TiO_2 and Nafion-coated TiO_2, Colloid Surf. A: Physicochem. Eng. Aspect 302 (2007) 261–268.
[29] Z.E. Allouni, M.R. Cimpan, P.J. Hol, T. Skodvin, N.R. Gjerdet, Agglomeration and sedimentation of TiO_2 nanoparticles in cell culture medium, Colloid Surf. B: Biointerf. 68 (2009) 83–87.
[30] P.K. Dutta, A.K. Ray, V.K. Sharma, F.J. Millero, Adsorption of arsenate and arsenite on titanium dioxide suspensions, J. Colloid Interf. Sci. 278 (2004) 270–275.
[31] P. Fernandez-Ibanez, J. Blanco, S. Malato, F.J. de las Nieves, Application of the colloidal stability of TiO_2 particles for recovery and reuse in solar photocatalysis, Water Res. 37 (2003) 3180–3188.
[32] K.A. Dunphy-Guzman, M.P. Finnegan, J.F. Banfield, Influence of surface potential on aggregation and transport of titania nanoparticles, Environ. Sci. Technol. 40 (2006) 7688–7693.
[33] Y.S. Ho, J.C.Y. Ng, G. McKay, Kinetics of pollutants sorption by biosorbents: review, Sep. Purif. Methods 29 (2) (2000) 189–232.
[34] A. Bahdod, S. El Asri, A. Saoiabi, T. Coradin, A. Laghzizil, Adsorption of phenol from an aqueous solution by selected apatite adsorbents: Kinetic process and impact of the surface properties, Water Res. 43 (2009) 313–318.
[35] D. Karadag, M. Turan, E. Akgul, S. Tok, A. Faki, Adsorption equilibrium and kinetics of reactive black 5 and Reactive Red 239 in aqueous solution onto surfactant-modified zeolite, J. Chem. Eng. Data 52 (2007) 1615–1620.
[36] E. Beyers, E. Biermans, S. Ribbens, K. De Witte, M. Mertens, V. Meynen, S. Bals, G. Van Tendeloo, E.F. Vansant, P. Pool, Combined TiO_2/SiO_2 mesoporous photocatalysts with location and phase controllable TiO_2 nanoparticles, Appl. Catal. B: Environ. 88 (2009) 515–524.
[37] V.K. Garg, R. Gupta, A.B. Yadav, R. Kumar, Dye removal from aqueous solution by adsorption on treated sawdust, Bioresour. Technol. 89 (2003) 121–124.
[38] I. Langmuir, Adsorption of gases on plain surfaces of glass mica platinum, JACS 40 (1918) 1361–1403.
[39] H. Freundlich, Über die adsorption in lösungen zeitschrift für Physikalische Chemie (Leipzig, 57 (1906) 384–470.
[40] M. Valix, W.H. Cheung, G. McKay, Roles of the textural and surface chemical properties of activated carbon in the adsorption of acid blue dye, Langmuir 22 (2006) 4574–4582.
[41] E. Lorenc-Grabowska, G. Gryglewicz, Adsorption characteristics of congo red on coal-based mesoporous activated carbon, Dyes Pigments 74 (2007) 34–40.
[42] S. Lagergren, Zur theorie der sogenannten adsorption gelöster stoffe, Kungliga Svenska Vetenskapsakademiens, Handlingar 24 (1898) 1–39.
[43] Y.S. Ho, G. McKay, The sorption of lead (II) ions on peat, Water Res. 33 (1999) 578–584.
[44] Y.S. Ho, G. McKay, Pseudo-second-order model for sorption processes, Process Biochem. 34 (1999) 451–465.
[45] X. Yang, B. Al-Duri, Kinetic modeling of liquid-phase adsorption of reactive dyes on activated carbon, J. Colloid Interf. Sci. 287 (2005) 25–34.
[46] M.A. Fontecha-Camara, M.V. Lopez-Ramon, L.M. Pastrana-Martinez, C. Moreno-Castilla, Kinetics of diuron and amitrole adsorption from aqueous solution on activated carbons, J. Hazard. Mater. 156 (2008) 472–477.
[47] W.J. Weber, J.C. Morris, Kinetics of adsorption on carbon from solution, J. Sanit. Eng. Div. ASCE 89 (1963) 31–60.
[48] A. Kumar, S. Kumar, S. Kumar, D.V. Gupta, Adsorption phenol and 4-nitrophenol on granular activated carbon in basal salt medium: Equilibrium and kinetics, J. Hazard. Mater. 147 (2007) 155–166.
[49] S. Al-Asheh, F. Banat, F. Abu-Aitah, Adsorption of phenol using different types of activated bentonites, Sep. Purif. Technol. 33 (2003) 1–10.
[50] S.J. Allen, G. McKay, K.Y.H. Khader, Intraparticle diffusion of a basic dye during adsorption onto sphagnum peat, Environ. Pollut. 56 (1989) 39–50.